Human Molecular Genetics, 2003, Vol. 12, No. 13 1555–1567
DOI: 10.1093/hmg/ddg169

Selective striatal neuronal loss in a YAC128 mouse model of Huntington disease

Elizabeth J. Slow[1], Jeremy van Raamsdonk[1], Daniel Rogers[1], Sarah H. Coleman[2], Rona K. Graham[1], Yu Deng[1], Rosemary Oh[1], Nagat Bissada[1], Sazzad M. Hossain[1], Yu-Zhou Yang[1], Xiao-Jiang Li[3], Elizabeth M. Simpson[1], Claire-Anne Gutekunst[2], Blair R. Leavitt[1] and Michael R. Hayden[1,*]

[1]Centre for Molecular Medicine and Therapeutics, Department of Medical Genetics, University of British Columbia, Vancouver, British Columbia, Canada V5Z 4H4, [2]Department of Neurology, Emory University, Atlanta, GA 30322, USA and [3]Department of Human Genetics, Emory University, Atlanta, GA 30322, USA

Received March 4, 2003; Revised and Accepted May 5, 2003

An expanded CAG repeat is the underlying genetic defect in Huntington disease, a disorder characterized by motor, psychiatric and cognitive deficits and striatal atrophy associated with neuronal loss. An accurate animal model of this disease is crucial for elucidation of the underlying natural history of the illness and also for testing experimental therapeutics. We established a new yeast artificial chromosome (YAC) mouse model of HD with the entire human HD gene containing 128 CAG repeats (YAC128) which develops motor abnormalities and age-dependent brain atrophy including cortical and striatal atrophy associated with striatal neuronal loss. YAC128 mice exhibit initial hyperactivity, followed by the onset of a motor deficit and finally hypokinesis. The motor deficit in the YAC128 mice is highly correlated with striatal neuronal loss, providing a structural correlate for the behavioral changes. The natural history of HD-related changes in the YAC128 mice has been defined, demonstrating the presence of huntingtin inclusions after the onset of behavior and neuropathological changes. The HD-related phenotypes of the YAC128 mice show phenotypic uniformity with low inter-animal variability present, which together with the age-dependent striatal neurodegeneration make it an ideal mouse model for the assessment of neuroprotective and other therapeutic interventions.

INTRODUCTION

The discovery of the gene responsible for Huntington's disease (HD) in 1993 facilitated the development of several genetic mouse models of this autosomal-dominant, neurodegenerative disease (1). Transgenic mouse models that expressed (in most cases) a truncated, N-terminal fragment of huntingtin under the control of a variety of promoters were the first models described (2–4). The replication of the underlying genetic defect, a CAG expansion, by inserting an expanded repeat into the murine huntingtin gene, led to the creation of 'knock-in' models (5–8).

Although the knock-in models accurately replicate the underlying genetic defect of HD, they do not present with robust motor deficits or demonstrate the brain atrophy and neuronal loss that characterize the human disease (5–8). In contrast, the truncated, N-terminal mice exhibit striatal atrophy and rapid onset of motor deficits (2,3). While a rapid-onset phenotype is beneficial for study, these truncated mice, by definition, lack the full-length huntingtin protein and therefore imperfectly replicate the protein context of the human condition.

We previously created a yeast artificial chromosome (YAC) mouse model of HD (9,10). Our goal was to establish a mouse model that expressed a full-length form of huntingtin under the control of the endogenous huntingtin promoter and regulatory elements. The YAC fulfilled both of these requirements, spanning the entire genomic region of the human HD gene, including promoter, intronic, upstream and downstream regulatory elements. The full-length, human huntingtin protein is expressed in a developmental and tissue-specific manner identical to the endogenous mouse protein (9,10).

We originally created YAC mice with 46 and 72 CAG repeats (mutant huntingtin mice) and YAC mice with 18 repeats in the

*To whom correspondence should be addressed at: Centre for Molecular Medicine and Therapeutics, 980 West 28th Avenue, Vancouver, BC, Canada V5Z 4H4. Tel: +1 6048753535; Fax: +1 6048753819; Email: mrh@cmmt.ubc.ca

HD gene (control mice) (10). These mice have helped elucidate different pathways involved in the pathogenesis of HD including increased susceptibility to excitotoxic cell death of neurons with mutant huntingtin (11–13), the discovery of decreased BDNF production in HD (14), the presence of mitochondrial dysfunction (15), and the anti-apoptotic role of wild-type huntingtin (16). However, the hyperactivity and neuronal degeneration in the YAC72 mice manifested late in the lifetime of the mouse (7 and 12 months, respectively) and the initial assessment of the HD-related phenotypes in these mice used predominantly qualitative measures (10). In addition, the presence of significant inter-animal variability in HD-related changes in the mice was a concern for assessing interventions which altered the natural history of the illness. Assessment of therapeutic interventions using YAC72 mice would require the use of large numbers of animals to determine a significant effect of an intervention at a significant cost. In an effort to create a YAC mouse with both an accelerated and quantifiable phenotype, and with the knowledge that increasing CAG repeat length leads to an earlier age of onset (17) and decreases variability (R. Brinkman and M.R. Hayden, manuscript in preparation), we created several YAC mouse lines with 128 CAG repeats (YAC128), and rigorously characterized one of these lines.

Our analysis of the YAC128 mice reveals a hyperkinetic phenotype first manifest at 3 months of age, followed by a progressive motor deficit on the rotarod present at 6 months with eventual progression to hypokinesis by 12 months of age. These behavioral changes are followed by striatal atrophy clearly evident by 9 months of age, cortical atrophy at 12 months and a progressive loss of striatal neurons accompanied by a decrease in striatal cell surface area. The motor deficit in the YAC128 mice is highly correlated with neuronal loss. The accurate replication of the human condition in the YAC128 mouse model, coupled with low inter-animal variability, results in an HD mouse model that is now highly suited for the assessment of different interventions on the disease phenotype.

RESULTS

Establishment of YAC128 Mice

A well-characterized YAC (353G6) spanning the entire HD gene including the promoter region was used to create the YAC128s (10). Homologous recombination was used to incorporate 128 CAG repeats obtained from PCR amplified, juvenile-onset HD patient DNA into the YAC in a previously described strategy (18). All founders were extensively screened by PCR and Southern blot as previously described (9). Two founders integrated the complete YAC and were used to establish two lines of YAC mice (lines 53 and 55) with 128 CAG repeats (Fig. 1A). Southern blots from these mice revealed that line 53 integrated more copies of the transgene than line 55 or line 2511, a previously described YAC72 mouse (10) (Fig. 1B). RNA analysis of the human huntingtin transcript demonstrated that line 53 had twice the RNA levels of line 55 and three times the RNA levels of line 2511 (Fig. 1C). Protein expression detected with HD650, a human huntingtin specific antibody, correlated exactly with RNA levels ($r^2 = 1.0$, Pearson correlation; Fig. 1E). Line 53 had the highest level of huntingtin protein expression (Fig. 1D) by densitometric analysis at approximately 75% of endogenous levels (data not shown). We further characterized line 53 due to the higher level of huntingtin protein expression.

Brain weight decrease in YAC128, line 53

Cohorts of line 53 mice (hereafter referred to as YAC128) and wild-type (WT) littermates at 6, 9 and 12 months were sacrificed and perfused and brain weight was measured. No difference in brain weight was detected in 6-month-old YAC128s ($WT = 0.421 \pm 0.016$ g, $YAC128 = 0.433 \pm 0.02$ g, $n = 5$; Fig. 2A). However, by 9 months of age YAC128 mice demonstrated a 5% decrease in mean brain weight compared with wild-type littermates ($WT = 0.414 \pm 0.016$ g, $YAC128 = 0.393 \pm 0.01$ g, $P < 0.05$; $n = 7$), progressing to a 10% decrease in 1-year-old YAC128s ($WT = 0.411 \pm 0.009$ g, $YAC128 = 0.373 \pm 0.022$ g, $P < 0.01$, $n = 7$; Fig. 2A). ANOVA analysis further revealed the effect of genotype ($F_{1,36} = 6.169$, $P = 0.018$), age ($F_{2,36} = 11.706$, $P = 0.0001$) and the interaction of age and genotype ($F_{2,36} = 5.002$, $P = 0.012$) on brain weight. The difference in brain weight did not appear to be due to generalized atrophy, but rather a region-specific effect. For example, no significant difference was detected between YAC128s and wild-type littermates in the weight of the cerebellum, a region not usually involved in HD pathology (19), at any of the ages examined (Fig. 2B).

Striatal and cortical volume is decreased in YAC128 mice

In order to determine whether the brain regions that are most affected in HD patients, the striatum and cortex (19,20), were also affected in YAC128 mice, striatal and cortical volume estimates of mice were calculated using stereological software. There was no detectable difference in striatal volume at 6 months of age in YAC128s compared with wild-type littermates ($WT = 14.3 \pm 2.39\,mm^3$, $YAC128 = 14.29 \pm 1.25\,mm^3$, $n = 5$; Fig. 3A). However, by 9 months of age, a 15% decrease in striatal volume was evident in YAC128 mice ($WT = 13.76 \pm 0.5\,mm^3$, $YAC128 = 11.81 \pm 0.36\,mm^3$, $P < 0.001$, $n = 7$; Fig. 3A), which was also seen in 12-month-old YAC128 mice ($WT = 11.27 \pm 0.68\,mm^3$, $YAC128 = 9.88 \pm 0.33\,mm^3$, $P < 0.01$, $n = 7$; Fig. 3A). Cortex volume was estimated from the region surrounding the crossing of the corpus callosum to the crossing of the anterior commissure (i.e. region of brain encompassing the greatest volume of striatum). In contrast to the striatum, there was no significant difference in cortical volume at 9 months of age ($WT = 14.43 \pm 0.79\,mm^3$, $YAC128 = 13.57 \pm 0.41\,mm^3$, $n = 5$) but a 7% decrease at 12 months of age ($WT = 12.83 \pm 0.50\,mm^3$, $YAC128 = 11.88 \pm 0.43\,mm^3$, $P < 0.05$, $n = 5$; Fig. 3B).

Neuronal loss and dysfunction in YAC128 mice

Striatal cell loss is a defining neuropathological characteristic of HD (21). Stereological software was used to estimate the striatal neuron number in our mouse cohorts. Sections were immuno-stained with NeuN, an antibody specific for a

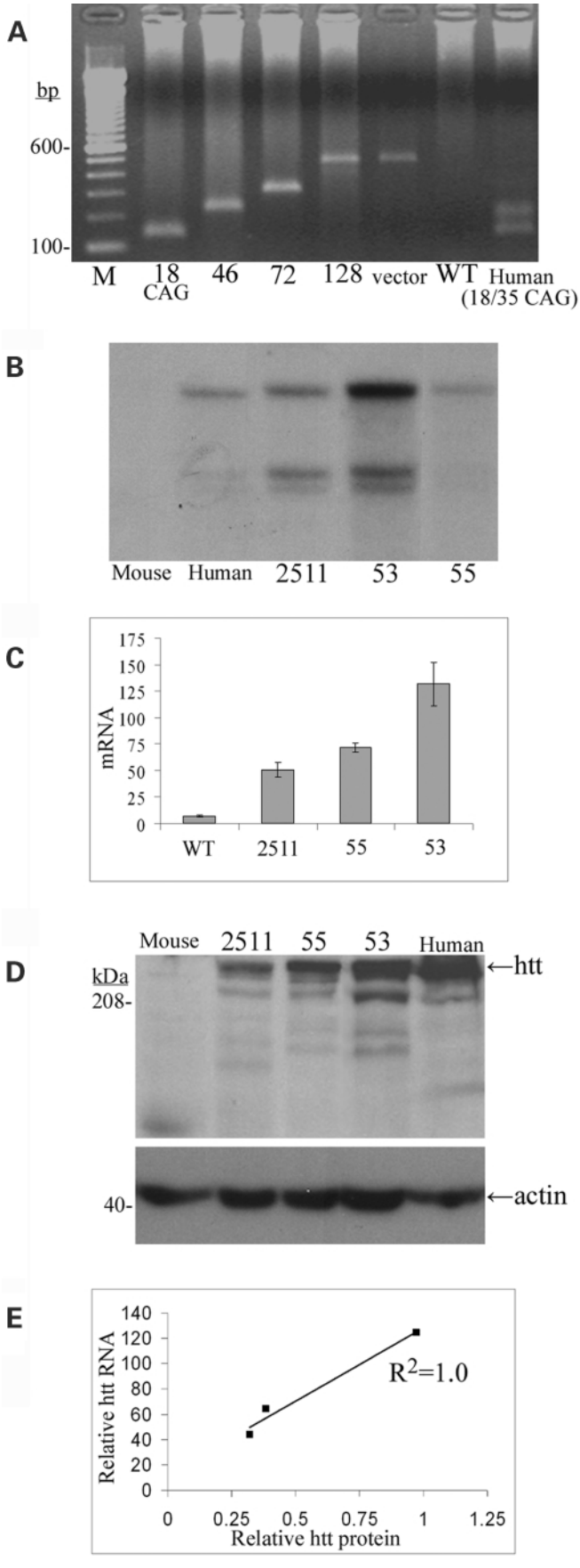

neuronal nuclear protein, which is present in most neuronal cell types (22). Counting of neurons, along with all other neuropathological and behavioral procedures, was performed completely blind with respect to genotype. At 9 months of age, YAC128 mice exhibited a decrease of 9% in striatal neuron count, although this trend did not reach significance ($P = 0.1$, $n = 3$; Table 1). To further examine neuronal loss at 9 months, the number of medium spiny neurons (MSNs), was assessed by immuno-staining for DARPP-32, a protein specific to MSNs (23). MSNs are the neurons that are most affected in HD (21) and are the major neuronal cell type of the striatum. YAC128 mice exhibited a decrease of 8% in MSN count, although this trend again did not reach significance ($P = 0.1$, $n = 7$; data not shown). Neuronal loss was progressive and by 12 months of age, a 15% decrease in striatal neuronal count was detected in the YAC128s compared with control littermates ($P < 0.01$, $n = 7$; Table 1). To ensure the validity of this finding, another group of YAC128 and control mice at 12 months of age underwent analysis. Similar to the previous results, the YAC128 mice in this group also exhibited an 18% decrease in striatal neuron count compared to controls ($P = 0.01$, $n = 5$; Table 1). There was no significant difference in neuronal density for the 9-month-old (WT $= 135500 \pm 1611$ neurons/mm^3), YAC128 $= 140700 \pm 3834$, $P = 0.28$) and 12-month-old (WT $= 138900 \pm 3927$, YAC128 $= 142500 \pm 2088$, $P = 0.43$) mouse cohorts. The lack of change in neuronal density combined with the loss in striatal volume of the YAC128 mice provides further evidence for neuronal loss in these mice.

We measured the cross-sectional area of the remaining striatal neurons to determine if the neurons were decreasing in size, a phenotype reported in other HD mouse models (4,24,25). The mean area of striatal neurons randomly selected by stereological software was decreased by 18% in 12-month-old YAC128s compared with controls (WT $= 65.71 \pm 4.5\,\mu m^2$, YAC128 $= 54.37 \pm 3.7\,\mu m^2$, $P < 0.01$, $n = 8$ animals), but not in 9-month-old YAC128s (WT $= 57.01 \pm 7.74\,\mu m^2$, YAC128 $= 60.62 \pm 4.76\,\mu m^2$, $n = 7$ animals; Fig. 4).

Figure 1. Characterization of YAC128 transgenic mouse. (A) Agarose gel showing CAG repeat expansion. PCR using human specific primers amplified the expanded CAG repeat from genomic DNA. The 18, 46 and 72 repeats were amplified from previously described YAC mice (9,10), while the 128 was amplified from a YAC128 mouse (line 53). The control (+ve) is from a yeast transfer vector with 128 CAGs. Wild-type (WT) mouse is a negative control and human DNA (18 and 35 CAGs) is another positive control. The marker is 100 bp ladder. (B) Southern blot for assessment of copy number. Genomic DNA digested with EcoR1 was probed with a human specific probe (CD70-2). Mouse DNA is the negative control, unaffected human is the positive control, previously described YAC72 (line 2511) and two lines of YAC128 (53,55) were assessed for copy number. (C) Real-time quantitative RT–PCR showing human huntingtin mRNA expression levels of YAC128. RNA was isolated from mouse frontal cortex. All PCR values are expressed as relative mRNA levels normalized to beta-actin mRNA levels. Error bars represent standard deviation from mean of $n = 3$ animals per group. (D) Western blot showing protein expression of YAC128. WT, lines 2511, 53, 55 and human control were probed with the human specific huntingtin antibody HD650. Blots were stripped and reprobed with anti-actin antibody to demonstrate equal loading. (E) Comparison of relative levels of human RNA and protein expression. Protein levels were calculated with NIH image densitometry software and normalized to actin. Pearson correlation revealed an $r^2 = 1.0$.

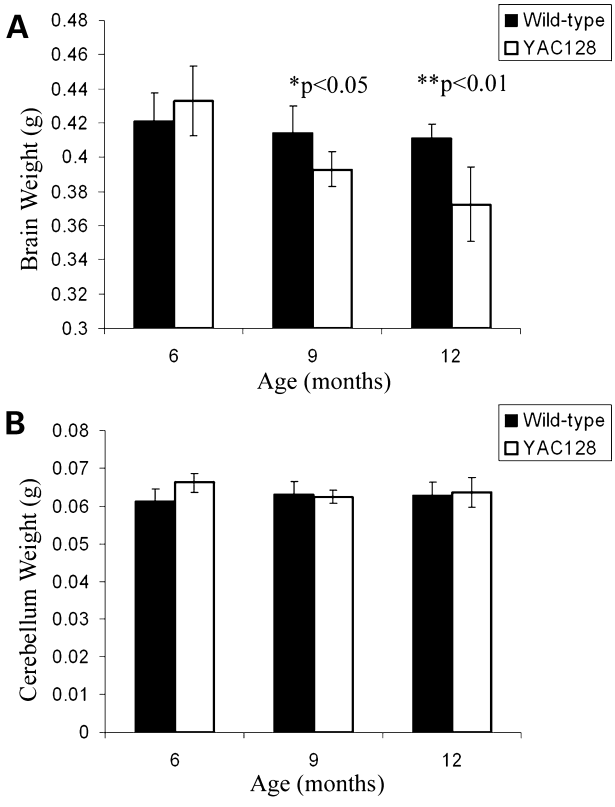

Figure 2. Brain weight is selectively decreased in YAC128 mice. (A) Perfused brain weight (including cerebellum) was compared between YAC128, line 53 and wild-type littermates at 6 (n = 5), 9 (n = 7) and 12 (n = 7) months of age. Brain weight in 9-month-old YAC128s was significantly decreased (*P < 0.05) and in 12-month-old YAC128s (**P < 0.01) by Student's t-test. Mean brain weight ± standard deviation of the groups is shown. (B) Cerebellum weight is not decreased in YAC128s. The cerebella were removed and weight was measured. There was no significant difference at any time point.

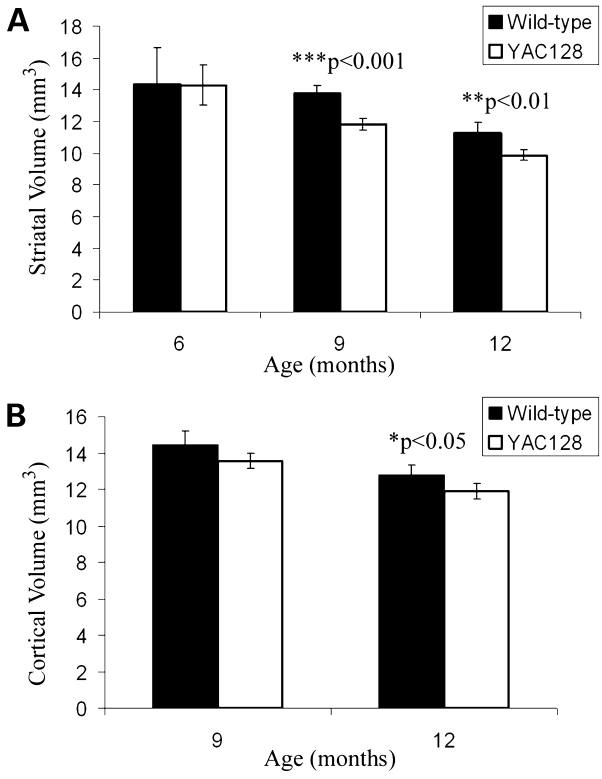

Figure 3. Striatal and cortical volume are decreased in YAC128 mice. Perfused brains were cut coronally into 25 µm sections throughout the striatum. Every eighth section was immuno-stained and Stereoinvestigator software was used to trace and calculate volume. (A) YAC128s showed no difference in striatal volume at 6 months (n = 5), a significant decrease at 9 months (n = 7, ***P < 0.001) and 12 months of age (n = 6, **P < 0.01) by Student's t-test. (B) Cortical volume was not significantly different at 9 months of age (n = 5) but decreased at 12 months of age (n = 5, *P < 0.05). Mean volume ± standard standard deviation for each group is shown.

Table 1. Striatal neuron number in YAC128 mice. Stereological software was used to assess the number of NeuN stained striatal neurons in serial sections of YAC128s versus controls. YAC128s showed a decrease in number of neurons at 12 months of age, but not at 9 months of age. The 12 month results were repeated in another set of animals.

Age (months)	WT	YAC128	n	Percentage decrease	Significance
9	1507000 ± 68530	1365000 ± 33580	3	9	NS, P = 0.16
12 (i)	1724000 ± 50270	1504000 ± 23640	7	15	P = 0.004
12 (ii)	1682000 ± 71870	1375000 ± 65360	5	18	P = 0.01

Behavioral assessment

YAC128 mice were studied at 3 month intervals from 3 to 12 months of age. Using an accelerating rotarod to examine fall latency, no difference in rotarod performance was detected between YAC128 and wild-type mice at 3 months (Fig. 5). However, by 6 months of age, a sharp decrease in rotarod performance was evident in YAC128 mice ($P < 0.01$), which was further decreased at 9 and 12 months of age ($P < 0.05$, $P < 0.01$ respectively; Fig. 5). ANOVA analysis further revealed the effect of genotype ($F_{1,28} = 6.77$, $P = 0.015$) and the interaction between genotype and age ($F_{3,84} = 4.662$, $P = 0.005$), indicating a significant difference in rotarod performance between wild-type and YAC128s with increasing age. ANOVA also reveals the highly significant effect of age ($F_{3,84} = 24.427$, $P < 0.001$) on rotarod performance for all mice.

Mouse activity was measured using an open-field apparatus for a period of 10 min at 3, 6, 9 and 12 months of age. ANOVA analysis showed a highly significant interaction between genotype and age in distance traveled ($F_{3,66} = 6.808$, $P < 0.001$), ambulatory counts ($F_{3,66} = 5.822$, $P = 0.001$), ambulatory episodes ($F_{3,66} = 6.698$, $P = 0.001$), time spent engaged in ambulatory movements ($F_{3,66} = 6.251$, $P = 0.001$), and time spent resting ($F_{3,66} = 2.409$, $P = 0.029$), revealing the significant difference in activity levels of wild-type and

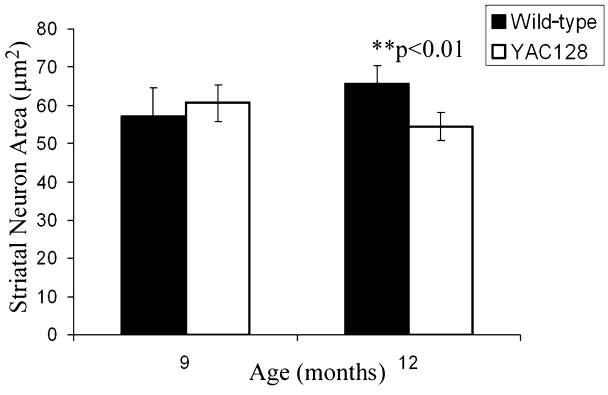

Figure 4. Striatal neuron surface area is decreased in YAC128 mice. Stereoinvestigator software randomly chose 50 × 50 μm frames within the striatum of a coronal section. The surface area of the neurons within the frames was calculated by the software (>70 neurons per animal). There is no difference in mean striatal neuron surface area in 9 month old YAC128s (n = 7 animals) but a significant decrease in surface area of striatal neurons in 12-month-old YAC128s (n = 6 animals, **P < 0.01) by Student's t-test. Mean striatal surface ± standard deviation for each group is shown.

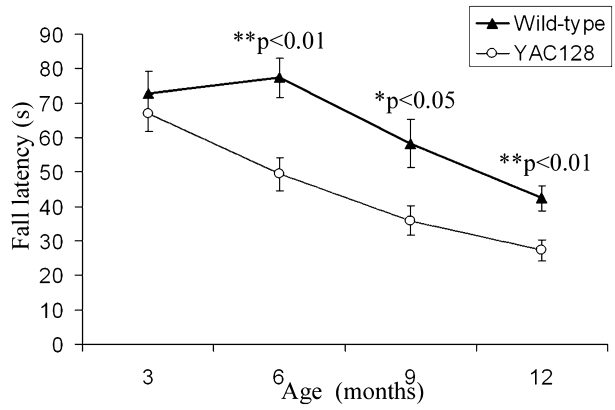

Figure 5. Rotarod deficit in YAC128 mice. YAC128s (n = 16) and wild-type control (n = 14) littermates were tested in three trials on an accelerating rotarod at 3 month intervals. At 3 months of age there was no difference between the two groups. At 6 months of age YAC128 rotarod performance had decreased (**P < 0.01). This deficit was present at 9 (*P < 0.05) and 12 months of age (**P < 0.01), although at these time points, wild-type mouse performance was also decreasing. ANOVA analysis revealed the significant interaction of genotype and time ($F_{3,84} = 4.662$, P = 0.005). Mean time spent on rotarod for each group is plotted and error bars represent SEM.

YAC128 mice overtime. At 3 months of age, the YAC128 mice exhibit a hyperkinetic phenotype compared with wild-type mice, illustrated by a significant elevation in distance traveled and ambulatory measurements and time spent in ambulatory movements (Fig. 6A–D). Interestingly, the YAC128s begin to manifest a hypokinetic phenotype at 6 months compared with wild-type littermates, and this hypokinetic phenotype is progressive with age, becoming significant by 12 months of age (Fig. 6A–E). To ensure the 10 min open field test was accurately measuring the activity of the mice, spontaneous locomotor activity was measured over a 24 h period in the home cage environment. Twelve-month-old YAC128 exhibited decreased activity compared with wild-type littermates (P < 0.01, n = 8; Fig. 6F), reproducing the results obtained in the 10 min analyses. YAC128 mice were heavier than their littermates at all ages examined (3, 6, 9 and 12 months). Since these mice overexpress full-length huntingtin, one possibility is the increased weight is due to the effects of full-length huntingtin on survival of cells (16,26).

Rotarod performance correlates with severity of neuronal loss

Five of the 12-month-old YAC128 mice analyzed for neuronal loss (Table 1) underwent rotarod assessment. Rotarod performance in this group of YAC128 mice was measured using a fixed speed rotarod, a testing paradigm shown to produce results that are highly correlative with results obtained using an accelerating rotarod in another mouse model of HD (27). YAC128 mice (n = 9) demonstrated decreased performance compared with wild-type controls at 40 rpm (P < 0.05) at 6 months of age, at 34 and 40 rpm (P < 0.05, P = 0.01) at 9 months and at 34 rpm (P < 0.001) at 12 months of age. Twelve-month-old mice from this study were analyzed for striatal volume, brain weight and striatal neuron count and, as shown in a separate analysis (Figs 2 and 3; Table 1), YAC128 mice exhibited reduced striatal volume, brain weight and neuronal loss. Five YAC128 mice were analyzed behaviorally at 6, 9 and 12 months and also neuropathologically at 12 months. A highly significant correlation was observed between rotarod performance at 12 months of age and striatal neuronal count (P < 0.01, $r^2 = 0.9214$; Fig. 7D). Mice with the greatest degrees of neuronal loss were associated with worsening performance on the rotarod. Clearly additional mice need to be analyzed to increase the power of this finding. Brain weight was also weakly correlated with rotarod performance (P < 0.05, $r^2 = 0.808$; Fig. 7E) and there was a trend towards a correlation between striatal volume and rotarod performance (P = 0.22, $r^2 = 0.442$; Fig. 7F). Interestingly, striatal neuronal loss was the most highly correlated of the three neuropathological measurements with rotarod performance. Because the mice were behavior tested over a period of months and only sacrificed for neuropathological measurements at 12 months, there was no neuropathological data for these mice at 6 or 9 months. However, the correlation between early rotarod performance and 12 month neuropathology could be examined. Interestingly, striatal neuronal count at 12 months of age was significantly correlated with rotarod performance at 6 months of age at 40 rpm ($r^2 = 0.8719$, P = 0.02; Fig. 7A) and at 9 months of age at 34 rpm (Fig. 7B; $r^2 = 0.9108$, P = 0.01) and 40 rpm ($r^2 = 0.7641$, P = 0.05; Fig. 7C), suggesting that early rotarod performance is predictive of the degree of ensuing neuronal loss.

Presence of aggregates

Brain sections from YAC128s were immuno-stained with EM48, an antibody that recognizes N-terminal huntingtin and is highly specific for aggregates (28). We observed increased nuclear huntingtin staining in 12-month-old YAC128s using brightfield microscopy but no nuclear huntingtin inclusions (n = 5; Fig. 8A). Huntingtin inclusions are defined as aggregates that are visible at the light microscope level. However, by electron microscopy many small clusters of three to six immunogold particles (micro-aggregates) are visible

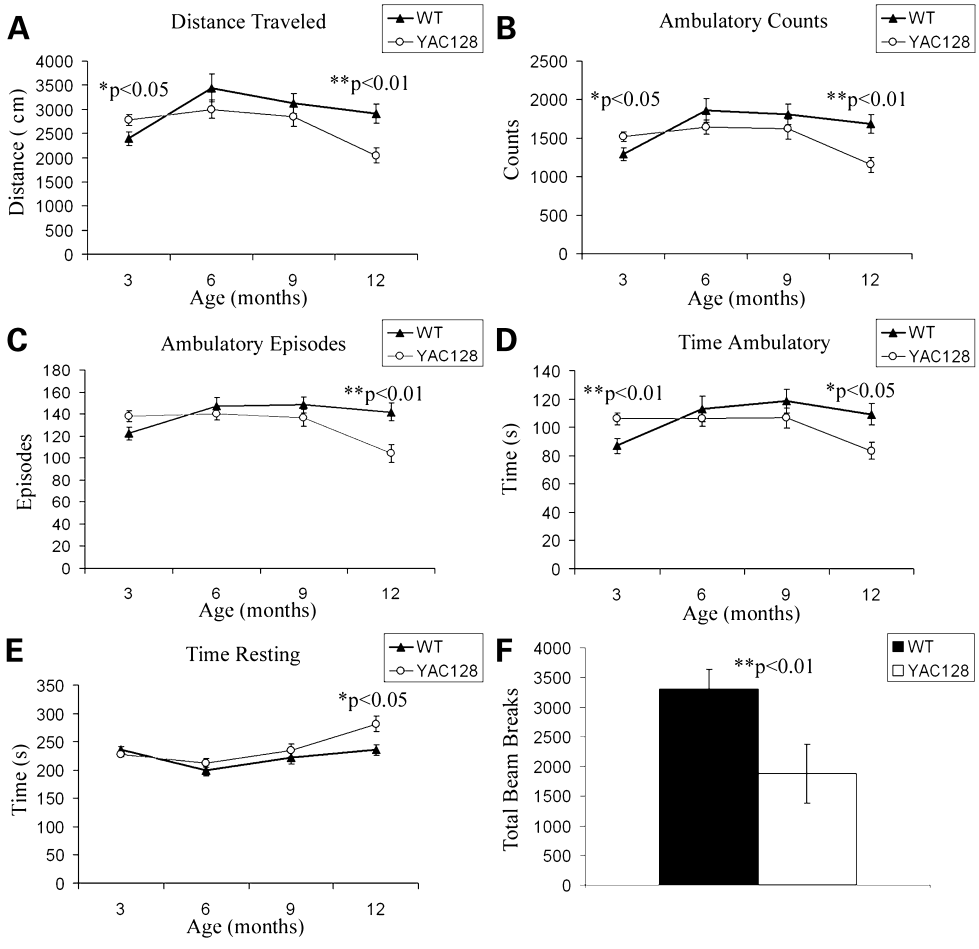

Figure 6. YAC128s initially exhibit hyperactivity followed by hypokinetic behavior. YAC128 (n = 14) and control (n = 12) (WT) littermates were tested in an open-field activity box over a period of 10 min. Five activity parameters were measured and the mean and standard error for the groups is shown. These measures include distance traveled (A), ambulatory counts (B), ambulatory episodes (C), time spent ambulating (D) and time spent resting (E). Locomotor activity was measured in the home cage environment over 24 h (n = 8 YAC128 and WT) (F). The mean measurement for each group is plotted and error bars represent SEM. Significant differences in group means by t-test are represented by asterisks and corresponding P-values.

throughout the nucleoplasm (Fig. 8D). EM48-positive inclusions were present in striatal cells of all 18-month-old YAC128s examined (Fig. 8B and C). By electron microscopy, these inclusions appeared as large clusters of immunogold particles (Fig. 8E and F). Wild-type animals did not exhibit nuclear huntingtin staining or inclusions at either 12 or 18 months (data not shown).

Low variability in the phenotypes of YAC128 mice

Lowering inter-animal variability decreases the number of animals necessary to determine a significant effect due to an experimental therapeutic and is likely to yield fewer false-negatives. As an indicator of variability, we looked at the number of YAC128 mice with measurements that had overlapping results with the wild-type control group. The decrease in striatal and cortical volume phenotype and the decrease in striatal neuron size phenotype showed no overlap between individual wild-type and YAC128 measurements (Table 2). By contrast, individual brain weights showed 33% overlap and the behavioral phenotype demonstrated 50% overlap between wild-type and single YAC128 mice. Using the data acquired in the characterization of the YAC128s, we performed a power analysis to estimate the number of animals we would need to detect a 33, 50 or 66% rescue at a significance of $P < 0.05$ with 80% power (Table 2). As variability increases, the number of animals necessary to determine a significant effect on that phenotype also rises. A small number of animals are required in a therapeutic trial where the goal is to determine a 50% rescue with the neuropathological phenotypes as endpoints, ranging from four animals for striatal volume to 13 animals for striatal neuronal loss. For a less effective rescue of 33%, only eight animals are required to determine a difference using striatal volume as an endpoint.

DISCUSSION

The YAC128 mouse represents a new animal model for HD, demonstrating motor deficit, a biphasic activity profile and

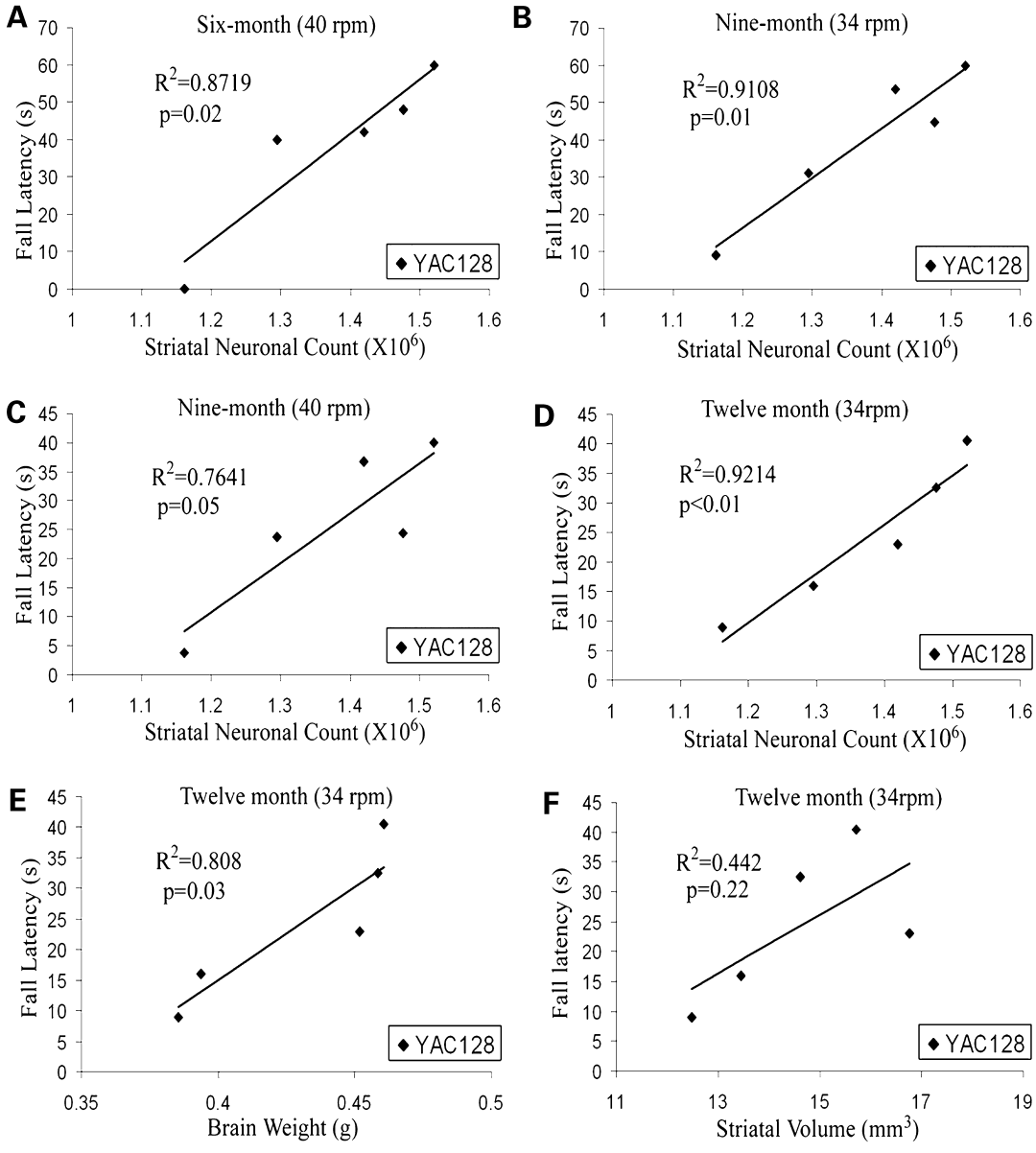

Figure 7. Impairment in rotarod activity is highly correlated with striatal neuronal loss. Rotarod performance at a fixed speed (34 or 40 rpm) was measured in 6-, 9- and 12-month-old YAC128 mice ($n = 5$) and correlated with neuropathological phenotypes using Pearson's correlation. Neuronal count at 12 months of age is significantly correlated with rotarod performance in 6-month old YAC128 mice at 40 rpm (A, $r^2 = 0.8719$, $P = 0.02$), 9-month-old YAC128 mice at 34 (B, $r^2 = 0.9108$, $P = 0.01$) and 40 rpm (C, $r^2 = 0.7641$, $P = 0.05$) and 12-month-old YAC128 mice at 34 rpm (D, $P < 0.01$, $r^2 = 0.9214$). Rotarod performance in 12-month old YAC128 mice is weakly correlated with brain weight (E, $P < 0.05$, $r^2 = 0.808$) and striatal volume (F, $P = 0.22$, $r^2 = 0.442$) at 12 months of age. Individual YAC128 mice are represented by diamond shapes.

Table 2. Overlap and power analysis for quantitative phenotypes in individual YAC128 mice. The number of YAC128 mice with measurements that overlap the measurements in the wild-type group is demonstrated. Power analysis determines the number of YAC128 animals necessary to detect a significant ($P < 0.05$) difference in treated versus untreated animals if you predict an 80% chance of discerning a 33, 50 or 66% rescue of the various quantitative phenotypes

Phenotype	Age (months)	Number of overlaps	Power		
			33% rescue	50% rescue	66% rescue
Striatal volume	9	0	8	4	2
Striatal neuron size	12	0	19	8	5
Brain weight	12	1/3	27	12	7
Striatal neuron count	12	1/8	30	13	7
Cortical volume	12	0	35	15	9
Rotarod	6	1/2	99	43	25

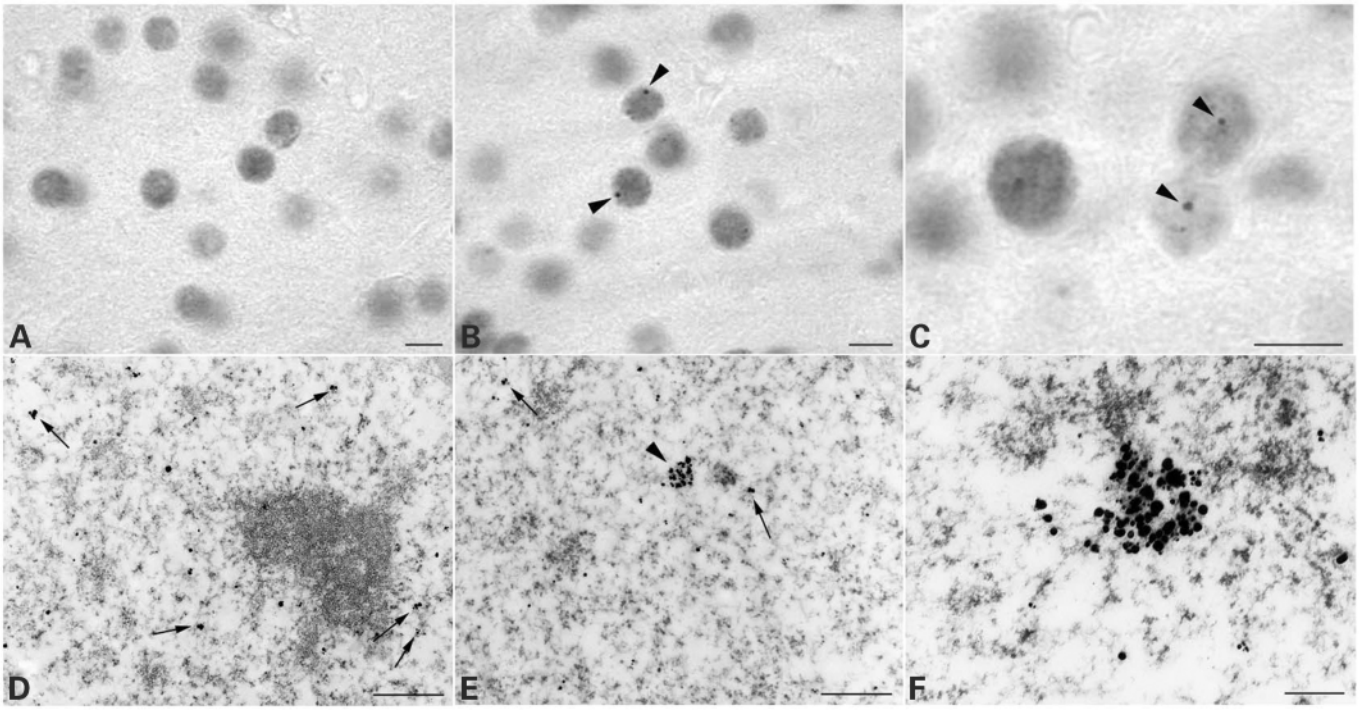

Figure 8. EM48 immunoreactivity in the striatum of 12- (A and D) and 18- (B, C, E and F) month-old YAC128 mice. At 12 months EM48 DAB reaction product is present in many nuclei (A). EM48 immunoreactivity is seen as diffuse staining as well as small EM48 positive puncta throughout the nucleoplasm. By electron microscopy many small clusters of three to six immunogold particles forming micro-aggregates are visible throughout the nucleoplasm (D, arrows). By 18 months, in addition to the diffuse staining and micro-aggregates, EM48 DAB reaction product is also seen in inclusions, visible as dark EM48 positive puncta by light level microscopy (B and C, arrowheads). By electron microscopy inclusions consist of large clusters of immunogold particles (F, arrows). Scale bars: A–C, 10 μm; D and E, 1 μm; F, 270 nm.

striatal atrophy associated with significant neuronal loss. The HD-related phenotypes exhibited in the YAC128 mouse model accurately recapitulates the changes observed in the human disease. Brain weight which is decreased in HD patients (19), and progressive neuronal (19,20) and volumetric loss in the striatum (29) is accurately mirrored in the YAC128 mice. A decrease in cortical volume, which occurs after the onset of striatal loss, also replicates the pathology and order of progression of the disease in human patients (21). Motor deficits are a hallmark of onset of HD in patients (19,20) and typically present before the onset of neurodegeneration (21). This natural history is replicated in the YAC128 model, with the onset of a motor deficit on the rotarod occurring before the onset of neuronal loss. Finally, the initial period of increased movement, evidenced by chorea and clumsiness, which generally progresses into a more rigid state as the disease progresses (20), parallels the biphasic activity profile of the YAC128s, composed of initial hyperactivity, followed by hypokinesis.

Other mouse models of HD have demonstrated varying degrees of striatal atrophy (2,4,8), brain weight loss (2) and motor deficit (3,4,30) exhibited in human patients. However, there are no reproducible reports of quantitative striatal neuronal loss, a hallmark of the human condition (19). Although the R6 truncated mouse models of HD have been reported to exhibit TUNEL staining in the striatum (31) and abnormal striatal neurons by toluidine blue staining (32), suggestive of apoptotic processes, quantitative loss of striatal neurons has not been reported. We observed a significant decrease in the number of striatal neurons in the YAC128 mouse model of HD. Qualitative observations of striatal neuronal degeneration, including nuclear shrinking, swelling of mitochondria and other features consistent with apoptosis, has been reported before in our YAC72 model (10).

A major question raised by this study is why is neuronal loss present in the YAC mice, but less evident in other models of HD? Neuronal loss is not specifically accounted for by the appropriate developmental and cell specific regulation of full-length huntingtin in the YAC model, as the mice with targeted insertion of expanded polyglutamine tracts into the endogenous mouse gene have similar regulation of the HD gene, but do not show the same degree of neuronal loss (5,7,8). The difference in striatal neuronal loss between the YAC mice and other knock-in animals also raises the possibility that human huntingtin with an expanded CAG tract is more toxic than the mouse gene with CAG expansion.

The unique finding of neuronal loss in the YAC mouse models compared with other HD mouse models may also be due (in part) to the differences in strains of the various models. An increasing body of evidence indicates a role for excitotoxic cell death in the striatal-specific neuron loss observed in HD (11–13). Excitotoxic lesions of rodent striatum caused by injections of kainic acid generate a neuropathological and behavioral phenotype that mimics the human condition (33,34). The background strain of the YAC mice is FVB/N, a strain that exhibits a high degree of neuronal loss when exposed to excitotoxic stress after injection of

kainic acid or quinolinic acid (35,36). In contrast, injection of excitotoxins into C57BL/6, the background strain common to most HD mouse models, results in a much lower degree of cell death relative to other mouse stains, including FVB, especially at low doses of kainic and quinolinic acid (35,36). Therefore, strain differences could account for differences in susceptibility to neurotoxicity of polyglutamine expansion.

The striatal neuronal loss observed in YAC128 mice is linearly correlated with the motor deficit assayed by rotarod. This intriguing result provides the first link in an animal model of HD between behavior and neuronal loss, suggesting a structural basis for the behavioral manifestations in the YAC128 mice. Interestingly, rotarod performance at 6 and 9 months of age is correlated with neuronal loss at 12 months of age. The degree of early motor dysfunction may therefore be an indicator of the severity of the extent of dysfunction of neurons present in the striatum; neurons that will eventually degenerate as the animal ages. The emergence of rotarod deficits, therefore, represents a time when neuronal dysfunction already has phenotypic effects, demonstrating the importance of assessing the effect of therapeutic interventions before and after this time point. The strong correlation between striatal neuronal loss and rotarod deficit suggests that neuronal loss and dysfunction are at least major contributors to the behavioral abnormalities in the YAC128 mice.

The characterization of the natural history in the YAC128 mice makes it an ideal model for defining the temporal relationship of other changes with striatal neuronal loss. Nuclear huntingtin inclusions visible under light microscopy are a common neuropathological marker in both human patients (28,37) and HD mouse models (3,6,10,38). The role of huntingtin inclusions in the pathogenesis of HD is still controversial. The appearance of huntingtin inclusions prior to the development of a neurologic phenotype in some transgenic models of HD suggested that the formation of these inclusions was potentially causative in the disease (38). However, in vitro experiments with mutant huntingtin demonstrated a distinct dissociation between the presence of huntingtin inclusions and huntingtin-related cell death (39,40). Studies in human patients showed little overlap between those cells exhibiting nuclear inclusions and the cells that undergo neurodegeneration in HD (28), further supporting the lack of correlation between inclusions and neuronal loss. Huntingtin inclusions are present in 18-month-old YAC128 mice, but not at 12 months of age, a time point when both behavioral and neuropathological changes, including neuronal loss, are present, demonstrating that inclusions are not involved in the initiation of neuronal loss. This finding corresponds with results previously observed in other mouse models of HD (8), demonstrating neuronal dysfunction before the onset of huntingtin inclusions. However, inclusion formation is believed to be the end stage of a process beginning with huntingtin translocation to the nucleus and continuing with the formation of micro-aggregates (38,41) visible under electron microscopy. Nuclear translocation and huntingtin micro-aggregates are present in 12-month-old animals, still leaving the question of the potential role of nuclear translocation and oligomerization of huntingtin as an initiating stimulus for HD earlier in the disease process.

The YAC mice will be useful for the assessment of therapeutic interventions, as this model accurately replicates the human disease and displays phenotypes that can be measured quantitatively with low inter-animal variability. The YAC128 mice exhibit progressive, quantitative phenotypes that parallel the human condition. The significance of low inter-animal variability in the use of a mouse model for therapeutic interventions is illustrated by the power analysis estimations. The phenotype with the lowest variability, striatal volume, requires only four animals to determine a 50% rescue at 9 months of age. Even the neuropathological phenotypes with greater variability (e.g. neuron count) require at most 13 animals to discern a 50% rescue. For a less robust therapeutic effect (33%), only eight animals are needed for assessment of striatal volume. This result demonstrates the potential usefulness of the YAC128 mice in therapeutic trials and the crucial importance of phenotypic predictability in a model used in experimental therapeutics.

The precise natural history of changes in the YAC128 mouse model of HD allows for further investigation of the temporal sequence and inter-relationships of other HD-related changes in the pathogenesis of the disease. The role of proteolytic cleavage of mutant huntingtin in the development of the disease is a question of particular interest. Increasing evidence implicates proteolytic cleavage of huntingtin by caspases (42), and/or calpains (43,44), and/or other unknown proteases (45) in the pathogenesis of HD. Caspase cleavage of mutant huntingtin leads to the formation of a toxic fragment of huntingtin (46) and this cleavage event is known to precede neurodegeneration in human patient brains (42). The expression of a full-length form of mutant huntingtin makes the YAC mouse model uniquely suited to test the efficacy of inhibition of these proteases on the disease development, either through the use of compounds, or through genetic manipulation. We can also use the YAC128 model to investigate the timing and effect of cortical dysfunction in the natural history of the disease. Results from mouse models (4) and other studies (14,42) implicate cortical dysfunction in striatal neuronal death in HD. Determining the timing of atrophy and neuronal loss in different layers and subsets of cortical tissue and the temporal relationship of this atrophy to striatal neuronal loss will further elucidate the role the cortex plays in the development of this devastating disease.

The YAC128 mouse model accurately recapitulates the striatal neuronal loss that characterizes the human disease, which allows the YAC128 mice to be useful in assessing experimental therapeutics that provide protection against neuronal loss. The defined natural history in YAC128 mice permits the accurate calculation of time points for commencement of therapeutic interventions, and endpoints for the assessment of the efficacy of those interventions. Using the data reported in this manuscript, we can now design experimental therapeutic trials with the YAC128 mice ensuring an adequate number of animals to properly assess the effect of neuroprotective strategies on the pathogenesis of HD.

MATERIALS AND METHODS

YAC mutagenesis and generation of mice

YAC mutagenesis was performed as described previously (10) using a construct containing 128 CAG repeats. YAC DNA was prepared for microinjection into FVB/N pronuclei, and founder

pups were screened (9). Mice were maintained on the FVB/N (Charles River, Wilmington, MA, USA) background strain and are congenic on this strain. Mice were genotyped by a PCR procedure described previously (9). Mice were housed, tested and tissues were harvested according to the University of British Columbia animal protocol A00-0254.

Copy number, RNA and protein analysis

Southern blotting to assess copy number was performed as described previously using 12 μg DNA (9) and the human specific probe cD70-2 (10).

Protein analysis. Protein lysates were prepared from whole mouse brain in a procedure described previously (9) with a caspase inhibitor, 10 μM ZVAD (Calbiochem, San Diego, CA, USA) added to the lysis buffer. These lysates were run on 7.5% polyacrylamide gels and blotted on PVDF membranes. Blots were probed with anti-actin (Chemicon, Temecula, CA, USA) and monoclonal antibody HD650. HD650 was produced against HD peptides 650–663 (VLRDEATEPGDQEN) and reacted specifically to human huntingtin. The HD peptides (VLRDEATEPGDNQEN) coupled to KLH carrier protein was used as an immunogen to inject Balb/C mice. The mouse was injected with 100 μg of the peptide-KLH protein in Freund's complete adjuvant subcutaneously, followed by two additional injections of 100 μg of the peptides-KLH protein in Freund's incomplete adjuvant at 14 day intervals. Three days before cell fusion, the mouse received an intravenous injection of 100 μg of the peptides via the tail vein. Splenocytes were fused with NS-1 myeloma cell, and hybridomas were selected and cloned in a procedure described previously (47).

RNA analysis. Total RNA was extracted from mouse cortex with RNeasy Protect Mini Kit (Qiagen, Mississauga, ON, Canada). First-strand cDNA was prepared from 1 μg of total RNA using SuperScript First-Strand Synthesis System for RT–PCR (Invitrogen, Burlington, ON, Canada) in a final volume of 20 μl. One in 100 of the RT reactions were used as template in real-time PCR reactions. Real-time PCR was performed using the ABI GeneAmp 5700 Sequence Detection System instrument and SYBR Green Two-step RT–PCR (Applied Biosystems, Foster City, CA, USA) using intron-spanning human specific primers. A dissociation curve confirmed the absence of nonspecific amplification. Serially diluted cDNA samples were used for standard curve calibration. All samples were run in quadruplicate. Expression levels were normalized to beta-actin mRNA levels. Primary data analysis was performed using system software from Applied Biosystems.

Morphological analysis

Mice were terminally anesthetized by intraperitoneal injection of 2.5% avertin and perfused with 3% paraformaldehyde/0.15% glutaraldehyde in PBS. The brains were left in the skulls for 24 h in 3% paraformaldehyde at 4°C, then removed and stored in PBS. Brains which did not perfuse well (softer than others) were removed from the groups at this point. We also removed two large brains from the analysis ($n = 1$ from the 9 month cohort, $n = 1$ from the 12 month cohort), which weighed 50–75% more than the other brains in the cohort and were significant outliers by Grubb's test. The genotype of all outliers was wild-type and the removal of these outliers did not affect the significance of the findings. Coronal sections of 25 and 50 μm thickness were cut throughout the striatum using a vibratome. Transgenic and wild-type mice were matched based on age and sex and littermates were used whenever possible.

Quantitative analysis

All quantitative analyses were performed blind with respect to genotype. Coronal sections (25 μm) spaced 200 μm apart throughout the striatum were stained with NeuN (Chemicon) antibody at 1:100 dilution or DARPP-32 antibody (Chemicon) at 1:500 dilution. Biotinylated secondary antibodies (Vector, Burlington, ON, Canada), mouse or rabbit at 1:200 were used prior to signal amplification with an ABC Elite kit (Vector) and detection with diaminobenzidine (DAB, Pierce). The perimeter of the striatum was traced in each of the serial sections using a 2.5× objective and Stereoinvestigator software (Microbrightfield, Williston, VT, USA). Subsequently, counts of neuronal profiles within 50×50 μm counting frames spaced evenly throughout the striatum (striatal grid size was 450×450 μm) was obtained using a 20× objective. Serial reconstruction of the striatum by the Stereoinvestigator software allowed estimation of total neuronal profiles and volume. Cortical volume was estimated in the region with the largest percentage of striatal tissue (centered on the landmarks of the corpus callosum and the anterior commisure crossing) totaling six serial sections. All layers and regions of cortex present in the section were outlined as a whole and volume was estimated using Neuroexplorer software (Microbrightfield, Williston, VT, USA). Cross-sectional area of striatal neuronal profiles was determined by outlining the perimeter of all clearly defined neurons within 50×50 μm counting frames spaced evenly throughout the striatum (450×450 μm grids). Neuronal profiles were outlined using a 100× objective in anatomically matched coronal sections. Note: tissue from wild-type and YAC128 at the same time point (e.g. 9 months) was treated identically; however, there was some experimental variability between time points (e.g. variability between tissue from 6 and 9 month time points), making volume comparisons between time points invalid.

Assessment of aggregates

Light microscopy. Brain sections of 25 μm thickness throughout the striatum were stained for the presence of aggregates. Sections were immuno-stained as described previously (28) using polyclonal EM48 antibody at 1:1000 and DAB as the chromogen (Vector).

Electron microscopy. For ultrastructural analysis, we used pre-embedding immunogold labeling of EM48. Sections were rinsed in PBS and processed according to manufacturer's instructions using EM48 antibodies at 1:500. Ultrasmall colloidal conjugated secondary antibody (Aurion, Wageningen, The Netherlands) was used to bind the primary antibody. Following a post-fixation with 2.5% gluteraldehyde, gold particles in

sections were intensified using R-gent SE-EM silver enhancement kit (Aurion, Wageningen, The Netherlands). Sections were then further fixed with 0.5% osmium tetroxide in 0.1 M PB for 15 min and processed for electron microscopy as described elsewhere (48). Selected sections were then placed in 0.5% osmium tetroxide in 0.1 M phosphate buffer for 30 min. Sections were then rinsed in PB, dehydrated in 25–100% EtOH followed by propylene oxide, infiltrated and flat embedded in Epon between sheets of Aclar and cured at 60°C for 2–3 days.

Behavioral assessment

Mice were singly housed in microisolator cages under reverse lighting (lights off at 11:00 a.m., lights on at 11:00 p.m.). All mice in a testing group were cage changed on the same day and no testing was performed until 2 days after a cage change. Mice were semi-randomly number coded from 1 to 40 (first and last half of testing group had an equal number of males/females, transgenic/wild-type). All behavioral testing was executed during the mouse night cycle, when the mice are normally active, with testing carried out in a behavioral testing suite under red light. The same observer carried out all of the tests and was blinded to the genotype of the individual mice throughout the course of the testing.

Rotarod analysis. We used an accelerating rotarod procedure where the rotarod (San Diego Instuments, San Diego, CA, USA) accelerated from 0 to 45 rpm over a period of 120 s. Mice were trained for 3 days with two trials per day on an accelerating rotarod. Following this training, the mice were tested for three consecutive trials in one day, with 1.5 h rest between trials. The rotarod was wiped clean with ethanol between each test subject.

Open-field analysis. Mice were assessed using an open-field activity monitor (Med Associates Inc., St Albans, VT, USA) for a period of 10 min. Testing began at least 1 h after the beginning of the mouse night cycle. The testing chamber was wiped clean with ethanol between each test subject. Ambulatory count was defined as the number of beam breaks while the mouse is ambulating, while ambulatory episodes are the number of times the mouse begins ambulating (from a resting position). Measurements were calculated by accompanying software (Med Associates). Mice who circled for the entirety of the 10 min interval were removed from the analysis ($n = 6$ wild-type, $n = 2$ YAC128).

Locomotor activity. Locomoter activity was measured for 24 h using a Cage Rack System (San Diego Instruments) with a uniformly spaced 8×4 photobeam grid. The cages were $28 \times 17 \times 12$ cm and the mice provided with food and water. Locomotor activity was calculated from the total number of beam breaks over the 24 h testing period.

Rotarod analysis—fixed speed. Mice were housed in microisolator cages with siblings. All behavioral testing was executed in the light in a behavioral testing suite. Mice were tested on a fixed speed rotarod (Ugo-Basile, Norfolk, UK) at 12, 24, 34 and 40 rpm and were initially trained at 24 rpm for 3 days with three trials per day. Subsequent testing occurred over a 3 day period, testing each speed once a day with 1.5 h rest in between tests. Mice were tested every month from 3 to 12 months of age.

Statistics

All statistics were carried out using an unpaired Student's t-test or two-way ANOVA with repeated measures. P-values, SEM, means and standard deviations were calculated using Graphpad Prism version 3.0 or Microsoft® Excel 2002. SPSS 11.5 was used to calculate F and P-values for behavioral measures. Correlation calculations with r^2 and P-values were calculated by Pearson correlation using Graphpad Prism version 3.0. Power analysis numbers were calculated using the website www.health.ucalgary.ca/~rollin/stats/ssize/n2.html.

Note

These mice are available for investigators for ongoing studies. Interested investigators should contact M.R.H.

ACKNOWLEDGEMENTS

The authors thank Hong Yi and the Emory Electron Microscopy Core at the Neurodegenerative Disease Center. We thank the Huntington Disease Society of America (HDSA), the Hereditary Disease Foundation (HDF) and Canadian Institutes of Health Research (CIHR) for support of this work to M.R.H. E.J.S., J.V.R. and R.K.G. are supported by CIHR studentships and the Michael Smith Foundation for Health Research. C.-A.G. is supported by the National Science Foundation. B.R.L. is supported by the HDF, CIHR and the Huntington's Society of Canada. E.M.S. is supported by Canada Foundation for Innovation and is a holder of a Canada Research Chair in Genetics and Behavior. M.R.H. is supported by a Merck Frosst grant to the CMMT, the CIHR, the Canadian Networks of Centers of Excellence, and is a holder of a Canada Research Chair in Human Genetics.

REFERENCES

1. Huntington's Disease Collaborative Research Group (1993) A novel gene containing a trinucleotide repeat that is expanded and unstable on Huntington's disease chromosomes. Cell, 72, 971–983.
2. Mangiarini, L., Sathasivam, K., Seller, M., Cozens, B., Harper, A., Hetherington, C., Lawton, M., Trottier, Y., Lehrach, H., Davies, S.W. and Bates, G.P. (1996) Exon 1 of the HD gene with an expanded CAG repeat is sufficient to cause a progressive neurological phenotype in transgenic mice. Cell, 87, 493–506.
3. Schilling, G., Becher, M.W., Sharp, A.H., Jinnah, H.A., Duan, K., Kotzuk, J.A., Slunt, H.H., Ratovitski, T., Cooper, J.K., Jenkins, N.A. et al. (1999) Intranuclear inclusions and neuritic aggregates in transgenic mice expressing a mutant N-terminal fragment of huntingtin. Hum. Mol. Genet., 8, 397–407.
4. Laforet, G.A., Sapp, E., Chase, K., McIntyre, C., Boyce, F.M., Campbell, M., Cadigan, B.A., Warzecki, L., Tagle, D.A., Reddy, P.H., Cepeda, C. et al. (2001) Changes in cortical and striatal neurons predict behavioral and electrophysiological abnormalities in a transgenic murine model of Huntington's disease. J. Neurosci., 21, 9112–9123.

5. Shelbourne, P.F., Killeen, N., Hevner, R.F., Johnston, H.M., Tecott, L., Lewandoski, M., Ennis, M., Ramirez, L., Li, Z., Iannicola, C. et al. (1999) A Huntington's disease CAG expansion at the murine Hdh locus is unstable and associated with behavioral abnormalities in mice. Hum. Mol. Genet., 8, 763–774.
6. Wheeler, V.C., White, J.K., Gutekunst, C.A., Vrbanac, V., Weaver, M., Li, X.J., Li, S.H., Yi, H., Vonsattel, J.P., Gusella, J.F. et al. (2000) Long glutamine tracts cause nuclear localization of a novel form of huntingtin in medium spiny striatal neurons in HdhQ92 and HdhQ111 knock-in mice. Hum. Mol. Genet., 9, 503–513.
7. Lin, C.H., Tallaksen-Greene, S., Chien, W.M., Cearley, J.A., Jackson, W.S., Crouse, A.B., Ren, S., Li, X.J., Albin, R.L. and Detloff, P.J. (2001) Neurological abnormalities in a knock-in mouse model of Huntington's disease. Hum. Mol. Genet., 10, 137–144.
8. Menalled, L.B., Sison, J.D., Wu, Y., Olivieri, M., Li, X.J., Li, H., Zeitlin, S. and Chesselet, M.F. (2002) Early motor dysfunction and striosomal distribution of huntingtin microaggregates in Huntington's disease knock-in mice. J. Neurosci., 22, 8266–8276.
9. Hodgson, J.G., Smith, D.J., McCutcheon, K., Koide, H.B., Nishiyama, K., Dinulos, M.B., Stevens, M.E., Bissada, N., Nasir, J., Kanazawa, I. et al. (1996) Human huntingtin derived from YAC transgenes compensates for loss of murine huntingtin by rescue of the embryonic lethal phenotype. Hum. Mol. Genet., 5, 1875–1885.
10. Hodgson, J.G., Agopyan, N., Gutekunst, C.A., Leavitt, B.R., LePiane, F., Singaraja, R., Smith, D.J., Bissada, N., McCutcheon, K., Nasir, J. et al. (1999) A YAC mouse model for Huntington's disease with full-length mutant huntingtin, cytoplasmic toxicity, and selective striatal neurodegeneration. Neuron, 23, 181–192.
11. Cepeda, C., Ariano, M.A., Calvert, C.R., Flores-Hernandez, J., Chandler, S.H., Leavitt, B.R., Hayden, M.R. and Levine, M.S. (2001) NMDA receptor function in mouse models of Huntington disease. J. Neurosci. Res., 66, 525–539.
12. Zeron, M.M., Chen, N., Moshaver, A., Lee, A.T., Wellington, C.L., Hayden, M.R. and Raymond, L.A. (2001) Mutant huntingtin enhances excitotoxic cell death. Mol. Cell Neurosci., 17, 41–53.
13. Zeron, M.M., Hansson, O., Chen, N., Wellington, C.L., Leavitt, B.R., Brundin, P., Hayden, M.R. and Raymond, L.A. (2002) Increased sensitivity to N-methyl-D-aspartate receptor-mediated excitotoxicity in a mouse model of Huntington's disease. Neuron, 33, 849–860.
14. Zuccato, C., Ciammola, A., Rigamonti, D., Leavitt, B.R., Goffredo, D., Conti, L., MacDonald, M.E., Friedlander, R.M., Silani, V., Hayden, M.R. et al. (2001) Loss of huntingtin-mediated BDNF gene transcription in Huntington's disease. Science, 293, 493–498.
15. Panov, A.V., Gutekunst, C.A., Leavitt, B.R., Hayden, M.R., Burke, J.R., Strittmatter, W.J. and Greenamyre, J.T. (2002) Early mitochondrial calcium defects in Huntington's disease are a direct effect of polyglutamines. Nat. Neurosci., 5, 731–736.
16. Leavitt, B.R., Guttman, J.A., Hodgson, J.G., Kimel, G.H., Singaraja, R., Vogl, A.W. and Hayden, M.R. (2001) Wild-type huntingtin reduces the cellular toxicity of mutant huntingtin in vivo. Am. J. Hum. Genet., 68, 313–324.
17. Brinkman, R.R., Mezei, M.M., Theilmann, J., Almqvist, E. and Hayden, M.R. (1997) The likelihood of being affected with Huntington disease by a particular age, for a specific CAG size. Am. J. Hum. Genet., 60, 1202–1210.
18. Duff, K., McGuigan, A., Huxley, C., Schulz, F. and Hardy, J. (1994) Insertion of a pathogenic mutation into a yeast artificial chromosome containing the human amyloid precursor protein gene. Gene Ther., 1, 70–75.
19. Harper, P. (1991) Huntington's Disease. W.B. Saunders, London.
20. Hayden, M.R. (1981) Huntington's Chorea. Springer, New York.
21. Vonsattel, J.P., Myers, R.H., Stevens, T.J., Ferrante, R.J., Bird, E.D. and Richardson, E.P. Jr (1985) Neuropathological classification of Huntington's disease. J. Neuropathol. Exp. Neurol., 44, 559–577.
22. Mullen, R.J., Buck, C.R. and Smith, A.M. (1992) NeuN, a neuronal specific nuclear protein in vertebrates. Development, 116, 201–211.
23. Ouimet, C.C., Langley-Guillon, K.C. and Greengard, P. (1998) Quantitative immunocytochemistry of DARPP-32-expressing neurons in the rat caudatoputamen. Brain Res., 808, 8–12.
24. Ferrante, R.J., Andreassen, O.A., Jenkins, B.G., Dedeoglu, A., Kuemmerle, S., Kubilus, J.K., Kaddurah-Daouk, R., Hersch, S.M. and Beal, M.F. (2000). Neuroprotective effects of creatine in a transgenic mouse model of Huntington's disease. J. Neurosci., 20, 4389–4397.
25. Levine, M.S., Klapstein, G.J., Koppel, A., Gruen, E., Cepeda, C., Vargas, M.E., Jokel, E.S., Carpenter, E.M., Zanjani, H., Hurst, R.S., et al. (1999) Enhanced sensitivity to N-methyl-D-aspartate receptor activation in transgenic and knockin mouse models of Huntington's disease. J. Neurosci. Res., 58, 515–532.
26. Dragatsis, I., Levine, M.S. and Zeitlin, S. (2000) Inactivation of Hdh in the brain and testis results in progressive neurodegeneration and sterility in mice. Nat. Genet., 26, 300–306.
27. Luesse, H.G., Schiefer, J., Spruenken, A., Puls, C., Block, F. and Kosinski, C.M. (2001) Evaluation of R6/2 HD transgenic mice for therapeutic studies in Huntington's disease: behavioral testing and impact of diabetes mellitus. Behav. Brain Res., 126, 185–195.
28. Gutekunst, C.A., Li, S.H., Yi, H., Mulroy, J.S., Kuemmerle, S., Jones, R., Rye, D., Ferrante, R.J., Hersch, S.M. and Li, X.J. (1999) Nuclear and neuropil aggregates in Huntington's disease: relationship to neuropathology. J. Neurosci., 19, 2522–2534.
29. Rosas, H.D., Goodman, J., Chen, Y.I., Jenkins, B.G., Kennedy, D.N., Makris, N., Patti, M., Seidman, L.J., Beal, M.F. and Koroshetz, W.J. (2001) Striatal volume loss in HD as measured by MRI and the influence of CAG repeat. Neurology, 57, 1025–1028.
30. Carter, R.J., Lione, L.A., Humby, T., Mangiarini, L., Mahal, A., Bates, G.P., Dunnett, S.B. and Morton, A.J. (1999) Characterization of progressive motor deficits in mice transgenic for the human Huntington's disease mutation. J. Neurosci., 19, 3248–3257.
31. Keene, C.D., Rodrigues, C.M.P., Eich, T., Chhabra, M.S., Steer, C.J. and Low, W.C. (2002) Tauroursodeoxycholic acid, a bile acid, is neuroprotective in a transgenic animal model of Huntington's disease. Proc. Natl Acad. Sci. USA, 99, 10671–10676.
32. Mastroberardino, P.G., Iannicola, C., Nardacci, R., Bernassola, F., De Laurenzi, V., Melino, G., Moreno, S., Pavone, F., Oliverio, S., Fesus, L. and Piacentini, M. (2002) 'Tissue' transglutaminase ablation reduces neuronal death and prolongs survival in a mouse model of Huntington's disease. Cell Death Differ., 9, 873–880.
33. Coyle, J.T. and Schwarcz, R. (1976) Lesion of striatal neurons with kainic acid provides a model for Huntington's chorea. Nature, 263, 244–246.
34. McGeer, E.G. and McGeer, P.L. (1976) Duplication of biochemical changes of Huntington's chorea by intrastriatal injections of glutamic and kainic acids. Nature, 263, 517–519.
35. Schauwecker, P.E. and Steward, O. (1997) Genetic determinants of susceptibility to excitotoxic cell death: implications for gene targeting approaches. Proc. Natl Acad. Sci. USA, 94, 4103–4108.
36. Schauwecker, P.E. (2002) Modulation of cell death by mouse genotype: differential vulnerability to excitatory amino acid-induced lesions. Exp. Neurol., 178, 219–235.
37. DiFiglia, M., Sapp, E., Chase, K.O., Davies, S.W., Bates, G.P., Vonsattel, J.P. and Aronin, N. (1997) Aggregation of huntingtin in neuronal intranuclearinclusions and dystrophic neurites in brain. Science, 277, 1990–1993.
38. Davies, S.W., Turmaine, M., Cozens, B.A., DiFiglia, M., Sharp, A.H., Ross, C.A., Scherzinger, E., Wanker, E.E., Mangiarini, L. and Bates, G.P. (1997) Formation of neuronal intranuclear inclusions underlies the neurological dysfunction in mice transgenic for the HD mutation. Cell, 90, 537–548.
39. Saudou, F., Finkbeiner, S., Devys, D. and Greenberg, M.E. (1998) Huntingtin acts in the nucleus to induce apoptosis but death does not correlate with the formation of intranuclear inclusions. Cell, 95, 55–66.
40. Kim, M., Lee, H.S., LaForet, G., McIntyre, C., Martin, E.J., Chang, P., Kim, T.W., Williams, M., Reddy, P.H., Tagle, D. et al. (1999) Mutant huntingtin expression in clonal striatal cells: dissociation of inclusion formation and neuronal survival by caspase inhibition. J. Neurosci., 19, 964–973.
41. Wheeler, V.C., Gutekunst, C.A., Vrbanac, V., Lebel, L.A., Schilling, G., Hersch, S., Friedlander, R.M., Gusella, J.F., Vonsattel, J.P., Borchelt, D.R. and MacDonald, M.E. (2002) Early phenotypes that presage late-onset neurodegenerative disease allow testing of modifiers in Hdh CAG knock-in mice. Hum. Mol. Genet., 11, 633–640.
42. Wellington, C.L., Ellerby, L.M., Gutekunst, C.A., Rogers, D., Warby, S., Graham, R.K., Loubser, O., van Raamsdonk, J., Singaraja, R., Yang, Y.Z. et al. (2002) Caspase cleavage of mutant huntingtin precedes neurodegeneration in Huntington's disease. J. Neurosci., 22, 7862–7872.
43. Kim, Y.J., Yi, Y., Sapp, E., Wang, Y., Cuiffo, B., Kegel, K.B., Qin, Z.H., Aronin, N. and DiFiglia, M. (2001) Caspase 3-cleaved N-terminal fragments of wild-type and mutant huntingtin are present in normal and Huntington's disease brains, associate with membranes, and undergo

calpain-dependent proteolysis. Proc. Natl Acad. Sci. USA, 98, 12784–12789.
44. Gafni, J. and Ellerby, L.M. (2002) Calpain activation in Huntington's disease. J. Neurosci., 22, 4842–4849.
45. Lunkes, A., Lindenberg, K.S., Ben-Haiem, L., Weber, C., Devys, D., Landwehrmeyer, G.B., Mandel, J.L. and Trottier, Y. (2002) Proteases acting on mutant huntingtin generate cleaved products that differentially build up cytoplasmic and nuclear inclusions. Mol. Cell, 10, 259–269.
46. Hackam, A.S., Singaraja, R., Wellington, C.L., Metzler, M., McCutcheon, K., Zhang, T., Kalchman, M. and Hayden, M.R. (1998) The influence of huntingtin protein size on nuclear localization and cellular toxicity. J. Cell Biol., 141, 1097–1105.
47. Davis, J.M., Pennington, J.E., Kubler, A.M. and Conscience, J.F. (1982) A simple, single-step technique for selecting and cloning hybridomas for the production of monoclonal antibodies. J. Immunol. Meth., 50, 161–171.
48. Gutekunst, C.A., Li, S.H., Yi, H., Ferrante, R.J., Li, X.J. and Hersch, S.M. (1998) The cellular and subcellular localization of huntingtin-associated protein 1 (HAP1): comparison with huntingtin in rat and human. J. Neurosci., 18, 7674–7686.